arXiv:1703.07501v1 [cond-mat.mes-hall] 22 Mar 2017

Skyrmions and Antiskyrmions in a Frustrated J_1-J_2-J_3 Ferromagnetic Film: Current-induced Helicity Locking-Unlocking Transition

Xichao Zhang,[1,2,*] Jing Xia,[1,*] Yan Zhou,[1,†] Xiaoxi Liu,[3] and Motohiko Ezawa[4,‡]

[1]*School of Science and Engineering, The Chinese University of Hong Kong, Shenzhen 518172, China*
[2]*School of Electronic Science and Engineering, Nanjing University, Nanjing 210093, China*
[3]*Department of Information Engineering, Shinshu University, 4-17-1 Wakasato, Nagano 380-8553, Japan*
[4]*Department of Applied Physics, The University of Tokyo, 7-3-1 Hongo, Tokyo 113-8656, Japan*

(Dated: March 23, 2017)

An intriguing feature of the magnetic skyrmion in a frustrated magnetic system is its helicity-orbital coupling. When the magnetic dipole-dipole interaction (DDI) is neglected, a skyrmion can show a current-induced rotational motion together with a helicity rotation since the energy is independent of the helicity. Here, we explore the skyrmion dynamics in a frustrated magnetic system based on the J_1-J_2-J_3 classical Heisenberg model explicitly by including the DDI. The skyrmion energy acquires a helicity dependence due to the DDI, resulting in a current-induced translational motion with a fixed helicity. The lowest energy states are the degenerate Bloch-type states with two distinguishable helicities, which could be used as information carriers in the binary memory. The skyrmion helicity can be identified by applying a small driving current as the direction of the translational motion is dependent of the helicity. It is found that by increasing the intensity of the driving current, the helicity locking-unlocking transition occurs, where the translational skyrmion motion with a fixed helicity changes to a rotational skyrmion motion together with a helicity rotation. This new aspect of the helicity-orbital coupling allows us to realize the flip of the helicity between two stable Bloch-type states by applying a strong current pulse, which could act as a switching process in the binary memory. Furthermore, we demonstrate that two skyrmions or two antiskyrmions can spontaneously form a bound state. We also show the separation of the bound state forced by a driving current. In addition, we show a pair annihilation of a skyrmion and an antiskyrmion accompanied with the emission of a propagating spin wave. Our results indicate the distinctive nature of skyrmions in frustrated magnetic materials, and also reveal unexpected properties of skyrmions which may lead to viable applications of topological spintronics.

PACS numbers: 75.10.Hk, 75.70.Kw, 75.78.-n, 12.39.Dc

The exotic and versatile magnetic skyrmion is a high-profile topological object in magnetic materials, which promises novel applications in spintronic devices[1–11]. The magnetic skyrmion was first experimentally identified in chiral magnetic materials in 2009[12]. After that, it has been experimentally observed, created, and modified in different systems, including magnetic materials[13–25], semiconductors[26], multiferroic materials[27], and ferroelectric materials[28]. Due to the properties of the topologically protected stability as well as the efficient mobility driven by external forces, the magnetic skyrmion is anticipated to be employed as the information carrier in future data storage devices[29–44], logic computing devices[45], microwave devices[46–48], spin-wave devices[49], and transistor-like devices[50,51].

Very recently, it is shown that the magnetic skyrmion in the frustrated magnetic system has remarkable physical properties that renovate our understanding of the chiral magnetic object[52–59]. Skyrmions in frustrated magnetic materials are stabilized by the quartic differential term, which is a reminiscence of the original mechanism of the dynamical stabilization proposed by Skyrme[60]. A prominent property is that a skyrmion and an antiskyrmion have the same energy irrespective to the helicity. For instances, the high-topological-number magnetic skyrmion[61] and the antiskyrmion[62] with the topological number of ± 2 are stable/metastable in the anisotropic frustrated magnet[52,53], where the magnetic skyrmion shows coupled dynamics of the helicity and the center of mass[53]. It is found that the translational motion of a magnetic skyrmion is coupled with its helicity in the frustrated magnet, resulting in the rotational skyrmion motion[52]. These novel properties due to the helicity-orbital coupling are lacking in the conventional ferromagnetic system, where the magnetic skyrmion is stabilized by the Dzyaloshinskii-Moriya interaction (DMI) and the helicity is locked.

In this paper, we explore skyrmions and antiskyrmions in a two-dimensional (2D) frustrated ferromagnetic system with competing exchange interactions based on the J_1-J_2-J_3 classical Heisenberg model on a simple square lattice[52]. We explicitly include the dipole-dipole interaction (DDI), which is neglected in the previous literature[52].

We first study the relaxed spin structure and the energy of a skyrmion with different initial values of the topological number and the helicity. The energies of a skyrmion with different helicity are degenerate in the absence of the DDI, but the degeneracy is resolved by the DDI. A skyrmion has two degenerate lowest energy states, which are the Bloch-type states with the helicities $\eta = \pm\pi/2$. Namely, a Bloch-type skyrmion has an internal degree of freedom taking a binary value of $\eta = \pm\pi/2$. These two Bloch-type skyrmions are clearly distinguishable since they move straight in opposite directions under a weak driving current. On the other hand, when a strong driving current is applied, the helicity is no longer locked, and the skyrmion performs a rotational motion together with a helicity rotation as if the DDI were absent.

We point out that it is possible to design a binary memory with the use of the binary helicity state of the Bloch-type skyrmion: (i) Apply a weak current pulse to a skyrmion at rest, and observe the direction of the motion (toward right or

left) to which a skyrmion begins to move; it determines the binary value of the skyrmion helicity: (ii) Apply a strong current pulse; it switches the binary value of the skyrmion helicity.

Furthermore, we demonstrate a spontaneous formation of the two-skyrmion bound state (the bi-skyrmion) as well as the two-antiskyrmion bound state (the bi-antiskyrmion) due to the attraction between two skyrmions and two antiskyrmions, respectively. Indeed, it is possible to split a bi-skyrmion as well as a bi-antiskyrmion by applying a driving current. The reason is that the direction of the skyrmion motion depends on its helicity. In addition, we demonstrate a pair annihilation of a skyrmion and an antiskyrmion, which emits a propagating spin wave upon the annihilation event. Our results indicate that there are more promising properties and degrees of freedom of skyrmions and antiskyrmions in the frustrated magnetic system, which have great potential to be used in future topological and spintronic applications.

Results

Theoretical model and simulations. We consider the J_1-J_2-J_3 classical Heisenberg model on a simple square lattice[52]. The Hamiltonian can be expressed as

$$\begin{aligned}\mathcal{H} = &- J_1 \sum_{<i,j>} \boldsymbol{m}_i \cdot \boldsymbol{m}_j - J_2 \sum_{\ll i,j \gg} \boldsymbol{m}_i \cdot \boldsymbol{m}_j \\ &- J_3 \sum_{\lll i,j \ggg} \boldsymbol{m}_i \cdot \boldsymbol{m}_j - H_z \sum_i m_i^z \\ &- K \sum_i (m_i^z)^2 + H_{\mathrm{DDI}}, \end{aligned} \tag{1}$$

where $\boldsymbol{m}_i$ represents the normalized spin at the site i, $|\boldsymbol{m}_i| = 1$. $\langle i,j \rangle$, $\langle\langle i,j \rangle\rangle$, and $\langle\langle\langle i,j \rangle\rangle\rangle$ run over all the nearest-neighbor (NN), next-nearest-neighbor (NNN), and next-next-nearest-neighbor (NNNN) sites in the magnetic layer, respectively. J_1, J_2, and J_3 are the coefficients for the NN, NNN, and NNNN exchange interactions, respectively. H_z is the magnetic (Zeeman) field applied along the $+z$-direction, K is the perpendicular magnetic anisotropy (PMA) constant, H_{DDI} represents the DDI, i.e., the demagnetization. The total energy of the given system contains the NN exchange energy, the NNN exchange energy, the NNNN exchange energy, the anisotropy energy, the Zeeman energy, and the demagnetization energy.

The simulation is carried out with the 1.2a5 release of the Object Oriented MicroMagnetic Framework (OOMMF) software[63]. The standard OOMMF extensible solver (OXS) objects are employed, including the OXS object for the calculation of the NN exchange interaction. In addition, we have developed the OXS extension modules for the calculation of the NNN and NNNN exchange interactions, which are implemented in our simulation of the J_1-J_2-J_3 classical Heisenberg model.

The time-dependent spin dynamics in the simulation is controlled by the Landau-Lifshitz-Gilbert (LLG) equation[63],

$$\frac{d\boldsymbol{m}}{dt} = -\gamma_0 \boldsymbol{m} \times \boldsymbol{h}_{\mathrm{eff}} + \alpha(\boldsymbol{m} \times \frac{d\boldsymbol{m}}{dt}), \tag{2}$$

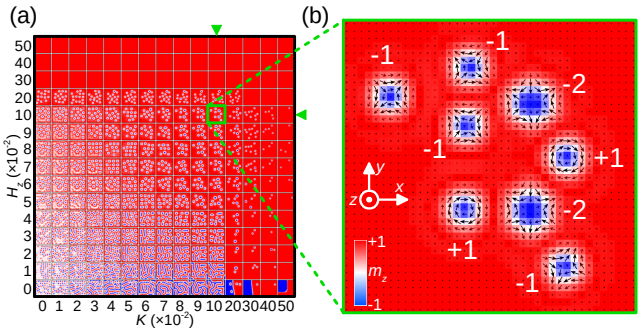

Figure 1. **Skyrmions and antiskyrmions in a frustrated J_1-J_2-J_3 ferromagnetic thin film.** (**a**) Phase diagram obtained by relaxing the magnetic thin film with a random initial spin configuration. (**b**) The spin configuration of the relaxed sample with $K = H_z = 0.1$, where both skyrmions and antiskyrmions are formed. The topological number Q is indicated. The color scale represents the out-of-plane spin component (m_z), which has been used throughout this paper. The arrow denotes the in-plane spin components (m_x, m_y). The simulation is carried out by the OOMMF CG minimizer. The model is a square element with the open boundary condition (OBC), which has 40×40 spins. The fixed parameters are $J_2 = -0.8J_1$ and $J_3 = -1.2J_1$. K and H_z are varied between $0 \sim 0.5$, respectively.

where $\boldsymbol{h}_{\mathrm{eff}} = -\partial\mathcal{H}/\partial\boldsymbol{m}$ is the effective field, t is the time, α is the Gilbert damping coefficient, and γ_0 is the gyromagnetic ratio. For the simulation including a vertical spin current generated by the spin Hall effect, the Slonczewski-like spin-transfer torque (STT) will be added to the right-hand side of equation (2),

$$\tau = -u\boldsymbol{m} \times (\boldsymbol{m} \times \boldsymbol{p}), \tag{3}$$

where $u = \frac{\gamma_0 \hbar j P}{2\mu_0 e a M_{\mathrm{S}}}$, j is the current density, $P = 0.4$ is the spin Hall angle, $a = 4$ Å is the lattice constant, M_{S} is the saturation magnetization, $\boldsymbol{p} = -\hat{y}$ is the spin-current polarization direction. Besides, we also employed the OOMMF conjugate gradient (CG) minimizer for the spin relaxation simulation, which locates local minima in the energy surface through direct minimization techniques[63].

In this work, the values for the NN, NNN, and NNNN exchange interactions are given as $J_1 = 3$ meV, $J_2 = -0.8J_1$, and $J_3 = -1.2J_1$, respectively. $K = 0 \sim 0.5J_1$, $H_z = 0 \sim 0.5J_1$, $\alpha = 0.1$, $\gamma_0 = 2.211 \times 10^5$ m A^{-1} s^{-1}, and $M_{\mathrm{S}} = 800$ kA m^{-1}. The geometry of the cubic cells generated by the spatial discretization is 4 Å × 4 Å × 4 Å.

We define the skyrmion number of a spin texture in the continuum limit by the formula

$$Q = -\frac{1}{4\pi} \int d^2\boldsymbol{r} \cdot \boldsymbol{m}(\boldsymbol{r}) \cdot (\partial_x \boldsymbol{m}(\boldsymbol{r}) \times \partial_y \boldsymbol{m}(\boldsymbol{r})) \,. \tag{4}$$

The normalized spin field $\boldsymbol{m}(\boldsymbol{r})$ takes a value on the 2-sphere S^2. The skyrmion number Q counts how many times $\boldsymbol{m}(\boldsymbol{r})$ wraps S^2 as the coordinate (x, y) spans the whole planar space. We parametrize the spin texture as

$$\boldsymbol{m}(\boldsymbol{r}) = \boldsymbol{m}(\theta, \phi) = (\sin\theta\cos\phi, \sin\theta\sin\phi, \cos\theta), \tag{5}$$

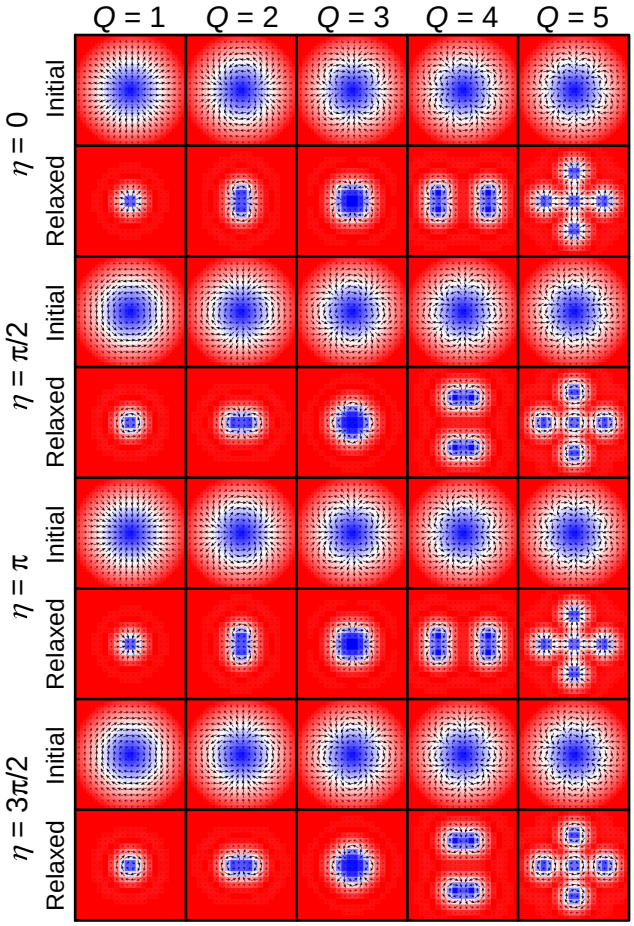

Figure 2. Relaxed states of skyrmions with different values of the skyrmion number Q and the helicity η. We construct a radial symmetric antiskyrmion as the initial state. We check whether the initial geometry is preserved or broken after the relaxation. The model is a square element with 40×40 spins. The parameters are $J_2 = -0.8J_1$, $J_3 = -1.2J_1$, $K = 0.1$, and $H_z = 0.1$. The simulation on the spin relaxation is carried out by the OOMMF CG minimizer.

with

$$\phi = Q\varphi + \eta, \tag{6}$$

where φ is the azimuthal angle ($0 \leq \varphi < 2\pi$) and η is the helicity defined mod 2π. Namely, the helicity η and $\eta - 2\pi$ are identical. Special values of the helicity play important roles, that is, $\eta = 0, \pi/2, \pi, 3\pi/2$. We frequently use $\eta = -\pi/2$ instead of $\eta = 3\pi/2$. We may index a skyrmion as (Q, η) with the use of the skyrmion number and the helicity. A skyrmion with $Q < 0$ may also be called an antiskyrmion.

Phase diagram. We first relax the frustrated magnetic system from a random initial spin configuration for different values of K and H_z. The initial spin configuration is random in three dimensions. The phase diagram of the relaxed state with respect to K and H_z is given in Fig. 1(a). It shows that isolated skyrmions and antiskyrmions can be spontaneously formed in the relaxed state where the magnetic system has certain values of K and H_z. Small values of K and H_z lead to to the formation of distorted skyrmions and antiskyrmion, or large in-plane spin configurations. Figure 1(b) shows the detailed spin configuration of the relaxed sample with $K = 0.1$ and $H_z = 0.1$. It can be seen that skyrmions with $(+1, -\pi/2)$, antiskyrmions with $(-1, \pi/2)$, $(-1, -\pi/2)$, and $(-2, \pi/2)$ coexist in the relaxed sample. It is noteworthy that the high-topological-number antiskyrmion with $Q = -2$ can be seen as a two-antiskyrmion bound state or a bi-antiskyrmion, about which we will discuss later.

Stability of isolated skyrmions and antiskyrmions. We study possible static solutions of isolated skyrmions and antiskyrmions by relaxing the sample with a given initial spin configuration. Namely, we construct a number of possible standard skyrmion and antiskyrmion spin structures with different values of (Q, η) as the initial spin configuration of the sample. After relaxation of the magnetic system, we get the relaxed states of skyrmions and antiskyrmions, which are stable or metastable solutions. As shown in Fig. 2, we construct a radial symmetric skyrmion as the initial state. We check whether the initial geometry is preserved or broken after the relaxation. For the initial states of skyrmions with $Q = \pm 1, \pm 2, \pm 3$, the numbers (Q, η) do not change after the relaxation although the radius shrinks. However the skyrmion with $Q = \pm 4$ is unstable and split into two skyrmions with $Q = \pm 2$. The helicity η changes during this splitting process from that of the initial state with $\eta = \pm\pi/2$. The skyrmion with $Q = \pm 5$ is also unstable and split into five skyrmions with $Q = \pm 1$ and different η. The results of the antiskyrmion are similar to those of the skyrmion as shown in the Supplementary Fig. 1.

Binary stable skyrmions and antiskyrmions. It has been demonstrated in Ref. 52 that the skyrmion energy and the antiskyrmion energy are degenerate and independent of the helicity η in the absence of the DDI. We also present a symmetric analysis of this property in Methods. Needless to say, the DDI exists in all magnetic materials. However, it has been customarily considered negligible for a microscopic spin texture. This is actually not the case. We show the detail of each contribution to the skyrmion energy in Fig. 3, where the DDI energy is found to be quite large.

As indicated in Fig. 4, there are two effects from the DDI. First, the degeneracy is resolved between the skyrmion and the antiskyrmion. Second, the degeneracy is resolved between various helicities in general. The Bloch-type (Néel-type) skyrmions with $\eta = \pm\pi/2$ ($\eta = 0, \pi$) are found to possess the minimum energy for $Q = \pm 1$ ($Q = \pm 3$). It is consistent with the fact that the DDI is due to the magnetic charge $\rho_{\text{mag}} = \nabla \cdot \boldsymbol{m}$ and prefers the Bloch-type structure[4]. On the other hand, the energy is independent of the helicity for $Q = \pm 2$. The helicity dependence of the energy of antiskyrmions is similar but weaker than that of skyrmions, as shown in Fig. 4(b). This is because an antiskyrmion has the antivortex structure, where the contribution of the DDI is smaller than the vortex structure of a skyrmion. The helicity dependence of the energy is a new feature due to the DDI,

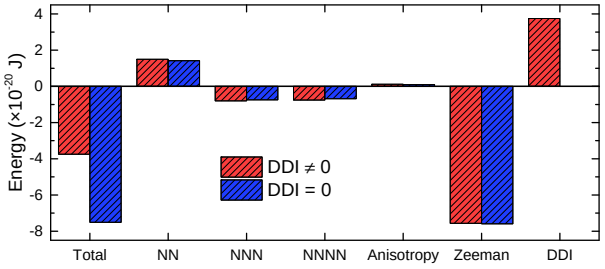

Figure 3. Details of the micromagnetic energy of a relaxed (1,$\pi/2$)-skyrmion in the presence and absence of the DDI. The contribution from the DDI energy is found to be quite large.

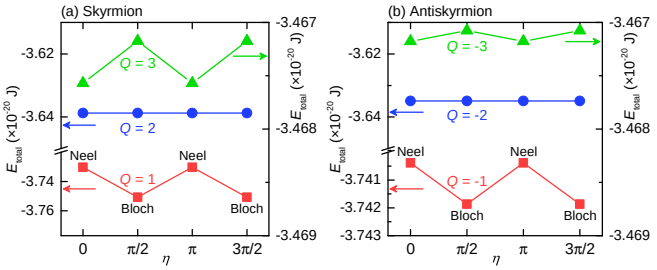

Figure 4. Total micromagnetic energy $E_{\rm total}$ for (a) relaxed skyrmions and (b) relaxed antiskyrmions as functions of the skyrmion number Q and the helicity η. $E_{\rm total}$ includes the NN exchange, NNN exchange, NNNN exchange, Zeeman, PMA, and DDI energies. The lowest energy states are found to be two degenerate Bloch states both for the skyrmion ($Q = 1$) and the antiskyrmion ($Q = -1$) due to the DDI. The corresponding spin configurations for relaxed skyrmions and antiskyrmions are given in Fig. 2 and Supplementary Fig. 1, respectively.

which is overlooked in the previous literature[52].

As a result, all skyrmions ($Q = \pm 1$) with any η relax to the Bloch-type skyrmions with $\eta = \pm\pi/2$ since they have the minimum energy. Exceptions are those possessing the precise initial values of $\eta = 0, \pi$. Indeed, we have studied the relaxation of a skyrmion with $(\pm 1, \eta)$ for different initial values of η in the range of $\eta = 0 \sim 2\pi$. As shown in Fig. 5, the skyrmion with the initial helicity of $\eta = 0, \pi/2, \pi, 3\pi/2$ keeps their helicity during the relaxation. However, for the skyrmion with other initial helicities, the helicity is relaxed to $\eta = \pm\pi/2$, justifying that the most stable skyrmions have $\eta = \pm\pi/2$. Consequently, the stable skyrmion is the Bloch-type skyrmion carrying the internal degree of freedom indexed by a binary value ($\eta = \pm\pi/2$).

Current-induced dynamics. A skyrmion and an antiskyrmion move rotationally together with a helicity rotation in the frustrated system without the DDI[52], as shown in Figs. 6(a) and 6(b). The skyrmion and antiskyrmion motions drastically change once the DDI is introduced. Indeed, the DDI produces the energy difference depending on the helicity as shown in Fig. 4. Namely, the helicity rotation costs some energies in the order of 0.01×10^{-20} J. In Fig. 5, we show the time evolution of the helicity. The helicity rotates toward that of the

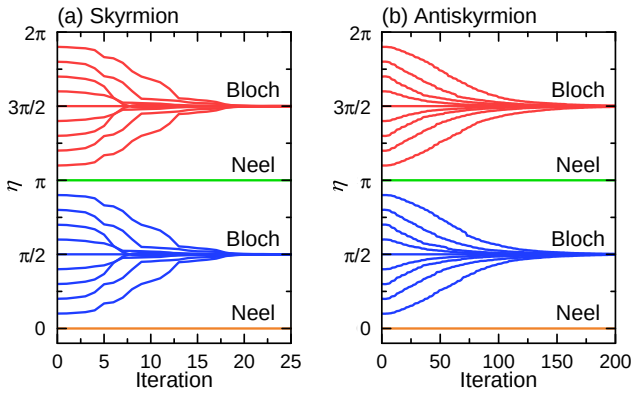

Figure 5. Helicity η as functions of the iteration for (a) skyrmions and (b) antiskyrmions with varied initial η. All of them are relaxed to the Bloch-type state unless they are initially in the Néel-type state. The model is a square element with 11×11 spins. The parameters are $J_2 = -0.8J_1$, $J_3 = -1.2J_1$, $K = 0.1$, and $H_z = 0.1$. The simulation on the spin relaxation is carried out by the OOMMF CG minimizer.

Bloch-type state ($\pm\pi/2$) unless the initial helicity is precisely of the Néel-type state.

This helicity locking occurs for the small driving current, since the Bloch-type skyrmion has the lowest energy in the presence of the DDI. Namely, under the small current injection, the helicity relaxes to that of the Bloch-type state, and then the skyrmion moves along a straight line with the helicity fixed, as shown in Fig. 6(c) and 6(d). This translational motion occurs due to the helicity locking by the DDI, which is highly contrasted to the case without the DDI.

However, as shown in Fig. 6(e) and 6(f), the translational motion with the fixed helicity turns out to be the rotational motion together with a helicity rotation once the intensity of the driving current exceeds a certain critical value (see Supplementary Figs. 2-4 and Supplementary Movies 1-2). The reason is that the energy injected by the current overcomes the potential difference between the Bloch-type and Néel-type skyrmions. Note that the current prefers the helicity rotation. This is the helicity locking-unlocking transition as a function of the intensity of the driving current.

Switching process of binary Bloch-type skyrmions. We have revealed prominent properties of the helicity-orbital coupling in the skyrmion motion in the frustrated magnetic system with the DDI. We may design a binary memory together with a switching process based on these properties. Let us start with a skyrmion at rest. (i) It is in one of the two Bloch-type states indexed by the helicity $\eta = \pm\pi/2$; since the helicity is a conserved quantity, we may use it as a one-bit memory. (ii) We can read its value by observing the motion of a skyrmion; when a small current pulse is applied, a skyrmion begins to move along a straight line toward left or right according to its helicity $+\pi/2$ or $-\pi/2$ [see Fig. 6(c) and Supplementary Movie 3]; this is the read-out process of the memory. (iii) On the other hand, when we apply a strong current pulse, a skyrmion begins to rotate together with its helicity

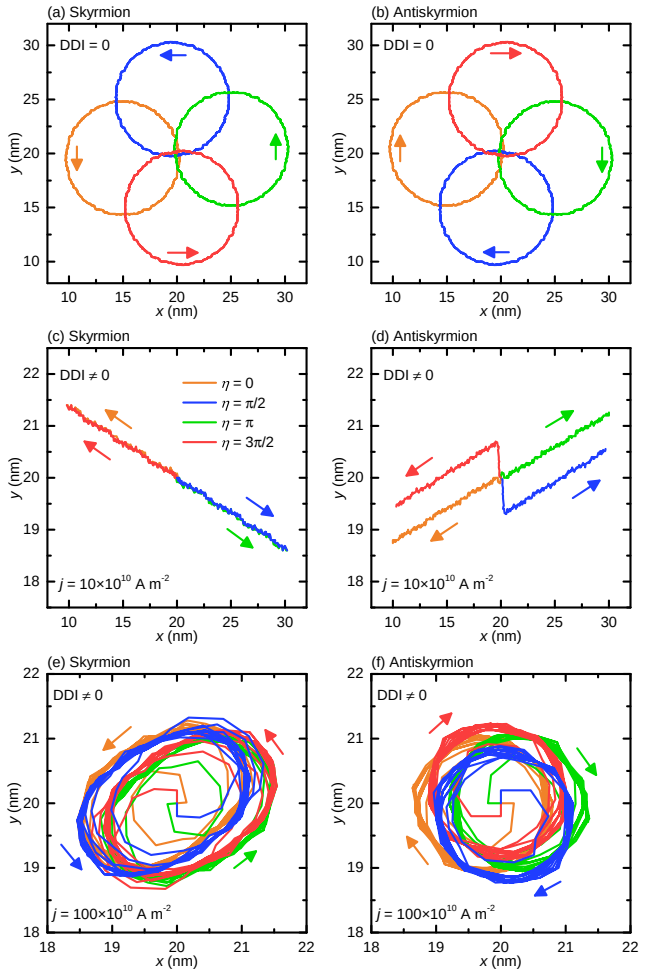

Figure 6. Trajectories of skyrmions and antiskyrmions in a frustrated J_1-J_2-J_3 ferromagnetic thin film. Trajectories of (**a**) skyrmions and (**b**) antiskyrmions with different initial helicities in the absence of the DDI. Trajectories induced by (**c**,**d**) a small driving current ($j = 10 \times 10^{10}$ A m^{-2}) and by (**e**,**f**) a large driving current ($j = 100 \times 10^{10}$ A m^{-2}) in the presence of the DDI. In the presence of the DDI, the skyrmion motion is along a straight line with the helicity fixed for the small driving current, but it is along a circle together with the helicity rotation for the large driving current. This is the helicity locking-unlocking transition. The model is a square element with 100×100 spins. The parameters are $J_2 = -0.8J_1$, $J_3 = -1.2J_1$, $K = 0.1$, $H_z = 0.1$, $\alpha = 0.1$. The simulation is carried out by the OOMMF solver integrating the LLG equation including the spin torque.

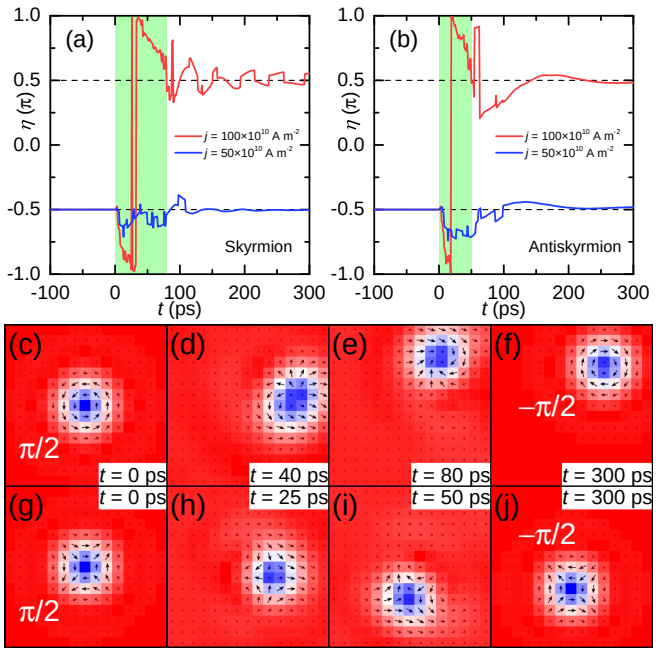

Figure 7. Flip of the skyrmion (antiskyrmion) helicity induced by a current pulse. (**a**) Skyrmion helicity as a function of time. A skyrmion is at rest with the helicity being $\eta = -\pi/2$. The helicity is flipped by a strong 80-ps-long current pulse and becomes $\eta = \pi/2$ (red curve). Such a flip does not occur by applying a small current pulse with the same duration (blue curve). (**b**) A similar flip occurs also for an antiskyrmion. (**c**)-(**f**) Snapshots of the skyrmion during the helicity flip process. (**g**)-(**j**) Snapshots of the antiskyrmion during the helicity flip process. The model is a square element with 39×39 spins. The parameters are $J_2 = -0.8J_1$, $J_3 = -1.2J_1$, $K = 0.1$, $H_z = 0.1$, and $\alpha = 0.1$. The simulation is carried out by the OOMMF solver integrating the LLG equation including the spin torque.

rotation; we can tune the pulse period to stop the helicity rotation so that it is relaxed to the flipped value of the initial helicity, as shown in Fig. 7. This is the switching process of the memory. As shown in Supplementary Movie 4, a skyrmion moving rightward is stopped and moves leftward after one rotation under a strong current pulse applied for an appropriate period.

Spontaneous formations of a bi-skyrmion and a bi-antiskyrmion. We proceed to investigate the spontaneous formations of a bi-skyrmion and a bi-antiskyrmion, that is, the spontaneous formations of a high-topological-number skyrmion and a high-topological-number antiskyrmion. We construct one skyrmion with $\eta = \pi/2$ and one skyrmion and $\eta = -\pi/2$, which are placed at the left and right sides of the sample, respectively, with the initial configuration as shown in Fig. 8. The dynamic process of the spontaneous formation of a bi-skyrmion is illustrated in Fig. 8(a), where a time-dependent relaxation of the system is simulated. The two skyrmions first move close to each other, where they both have in-plane spins near each other that are pointing along the $+y$-direction. The two skyrmions then smoothly merge into one bi-skyrmion with $Q = +2$, when the encountered in-plane spins are rotated into the $+z$-direction. Finally, a bi-skyrmion with $Q = +2$ is formed in the sample (see Supplementary Movie 5). A similar spontaneous formation of a bi-antiskyrmion with $Q = -2$ is possible as given in Fig. 8(b) (see Supplementary Movie 6).

The natural and spontaneous formations of a bi-skyrmion and a bi-antiskyrmion are caused by the skyrmion-skyrmion attraction and the antiskyrmion-antiskyrmion attraction, respectively. A detailed analysis on the interactions among skyrmions and antiskyrmions is given in Supplementary

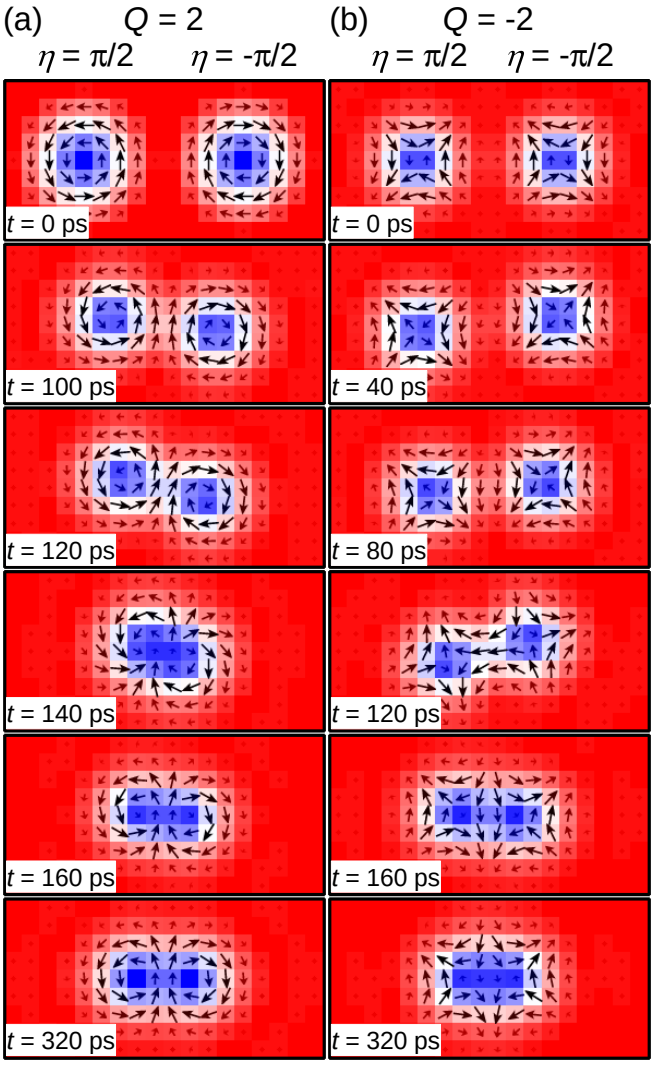

Figure 8. Spontaneous formations of a bi-skyrmion and a bi-antiskyrmion. (**a**) Spontaneous formation of a bi-skyrmion by merging two skyrmions and different η. (**b**) Spontaneous formation of a bi-antiskyrmion by merging two antiskyrmions and different η. The model is a square element with 18×9 spins. The parameters are $J_2 = -0.8J_1$, $J_3 = -1.2J_1$, $K = 0.1$, $H_z = 0.1$, and $\alpha = 0.1$. The simulation is carried out by the OOMMF solver integrating the LLG equation.

Figs. 5-8. On the other hand, it is noteworthy that the helicity rotation of the antiskyrmion is caused by the coupling between the translational motion and the helicity, as reported in Ref. 52. The rotation of the helicity also happens for the skyrmion, although it is not obvious in Fig. 8(a) as the spacing between the two skyrmions is very short.

Forced separations of a bi-skyrmion and a bi-antiskyrmion. After showing the spontaneous formations of the bi-skyrmion and the bi-antiskyrmion, we further demonstrate that it is possible to split the bi-skyrmion and the bi-antiskyrmion by applying a driving current.

Figure 9 demonstrates the forced separation of two skyrmions from a bi-skyrmion. We first place a relaxed bi-skyrmion at the center of the sample. Then, a driving current of $j = 8 \times 10^{11}$ A m^{-2} is vertically injected to the sample, which can be realized by the spin Hall effect in a heavy-metal substrate. It is found that the bi-skyrmion starts to rotate counterclockwise, and forms a clear peanut-like shape, as shown in Fig. 9(f). When it has rotated almost 180 degrees, two skyrmions are almost generated, as shown in Fig. 9(k). As shown in Fig. 9(l), the bi-skyrmion is successfully split into two isolated skyrmions (see Supplementary Movie 7). This forced separation is possible since the bi-skyrmion is composed of two skyrmions with opposite helicities, which rotate in opposite directions. The separation process of a bi-antiskyrmion forced by the driving current is similar to that of the bi-skyrmion (see Supplementary Fig. 9 and Supplementary Movie 8).

We note that the total skyrmion number conserves during both the spontaneous formation and the forced separation of the bi-skyrmion and the bi-antiskyrmion. Furthermore we found that the bound state with a higher skyrmion number $|Q| > 2$ can also be spontaneously generated (see Supplementary Figs. 10 and 11).

Pair annihilation of a skyrmion and an antiskyrmion. Finally, we demonstrate that the pair annihilation process of a skyrmion and an antiskyrmion in a forced collision event driven by the current, as shown in Fig. 10. We first place a relaxed skyrmion and a relaxed antiskyrmion at the center of the sample. There is a certain spacing between the skyrmion and the antiskyrmion. Then, a 200-ps-long driving current pulse of $j = 8 \times 10^{11}$ A m^{-2} is vertically injected to the sample. The skyrmion and the antiskyrmion move in a circular trajectory toward opposite directions. The helicity η of the skyrmion and the antiskyrmion varies with the position as it is coupled with the orbital motion (see Fig. 6 and Ref. 52). As shown in Fig. 10(b), the skyrmion meets the antiskyrmion, where the skyrmion has the helicity of $\eta = \pi/2$ while the antiskyrmion has the helicity of $\eta = -\pi/2$, which is the condition for the pair annihilation. The skyrmion and the antiskyrmion then form a magnetic bubble state with $Q = 0$, as shown in Fig. 10(d). The magnetic bubble state, which is not topologically protected, rapidly shrinks in size and is finally evolved into the trivial ground state, as shown in Fig. 10(l). This is the exact process of the pair annihilation of a skyrmion and an antiskyrmion (see Supplementary Movie 9). A forced collision between a skyrmion and an antiskyrmion will lead to the pair annihilation of the skyrmion and the antiskyrmion as long as they do not have identical η (see Supplementary Fig. 8). It is also worth mentioning that a propagating spin wave is emitted during the pair annihilation, which can be discerned from Fig. 10.

Discussion

We have studied magnetic skyrmions in a 2D frustrated magnetic system with competing exchange interactions based on the J_1-J_2-J_3 classical Heisenberg model on a simple square lattice. We have demonstrated that the contribution of the DDI energy is significant although the scale of a skyrmion is of the

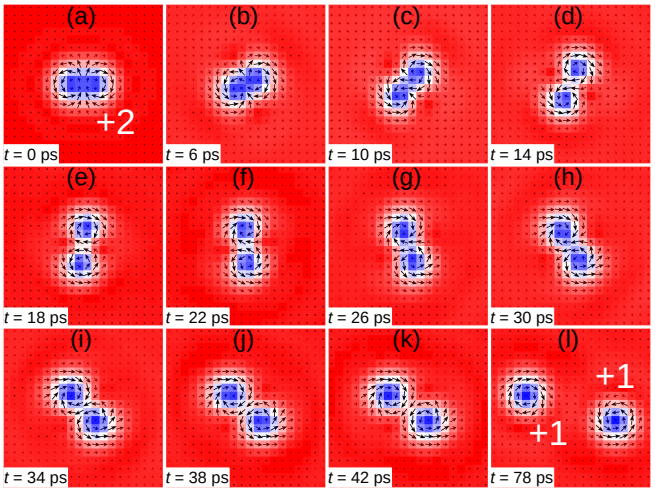

Figure 9. **Forced separation of two skyrmions from a bi-skyrmion with $Q = 2$.** (a) We first place a relaxed bi-skyrmion. (b) It starts to rotate counterclockwise under an injected driving current. After forming a clear peanut-like shape, it is separated into two skyrmions as in (l). The model is a square element with 40×40 spins. The parameters are $J_2 = -0.8J_1$, $J_3 = -1.2J_1$, $K = 0.1$, $H_z = 0.1$, $\alpha = 0.1$, and $j = 8 \times 10^{11}$ A m^{-2}. Q is indicated in (a) and (l). The simulation is carried out by the OOMMF solver integrating the LLG equation including the spin torque.

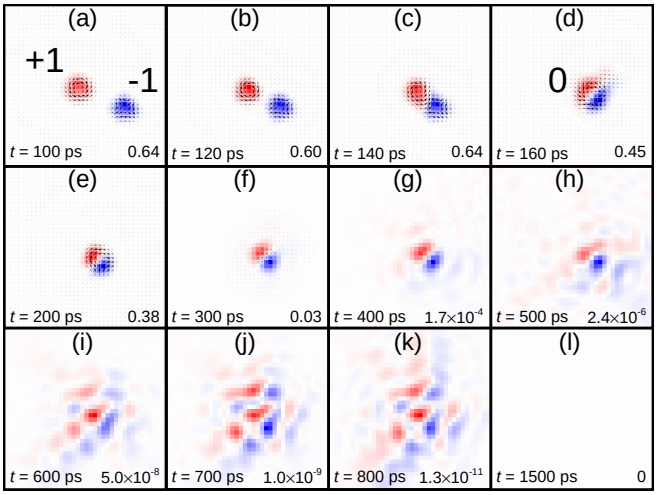

Figure 10. **Pair annihilation of a skyrmion and an antiskyrmion.** (a) We first place a skyrmion and an antiskyrmion. (d) They are spontaneously combined into a magnetic bubble ($Q = 0$). Then, by emitting spin waves, it disappears. The spin wave can be discerned from (**g**)-(**k**). The positive and negative skyrmion number densities are denoted by red and blue colors, respectively. Q is indicated in (**a**) and (**d**). The maximum value of the Q density is indicated in the lower right corner of each snapshot. The model is a square element with 60×60 spins. The parameters are $J_2 = -0.8J_1$, $J_3 = -1.2J_1$, $K = 0.1$, $H_z = 0.1$, $\alpha = 0.1$, and $j = 8 \times 10^{11}$ A m^{-2}.

order of nanometer. As a result, the Bloch-type skyrmion has the lowest energy and is stabilized. It has a bistable structure indexed by the helicity $\eta = \pm\pi/2$.

The role of the helicity-orbital coupling becomes remarkable in the presence of the DDI. First, a skyrmion moves along a straight line with a fixed helicity under a week driving current. The moving direction of a skyrmion is opposite when its helicity is opposite. Second, the dynamics of a skyrmion drastically changes from the translational motion to the circular motion as the increase of the driving current, which is the locking-unlocking transition of the helicity. Third, we can flip the helicity of a skyrmion by applying a strong current pulse with a reasonable period. We have argued that these properties could be used to design a binary memory together with read-out process as well as the switching process.

Furthermore, we have shown that magnetic skyrmions with $Q = \pm 1, \pm 2, \pm 3$ are possible metastable topological nontrivial states in the frustrated magnetic system. The skyrmion with a high topological number $|Q| > 1$ could be seen as a bound state or a cluster of skyrmions. In particular, we have demonstrated the spontaneous formation and the forced separation of a bi-skyrmion. In addition, we have shown the pair annihilation of a skyrmion and an antiskyrmion by triggering a collision event.

Our results reveal the exotic and promising properties of skyrmions and antiskyrmions in the frustrated magnetic system, which may lead to novel spintronic and topological applications based on the manipulation of skyrmions and antiskyrmions.

Methods

Symmetry analysis. A skyrmion is indexed by the skyrmion number Q and the helicity η. We study how the helicity is fixed by minimizing the Hamiltonian. First, we examine the Hamiltonian equation (1), which is rewritten as

$$H = -\frac{1}{2}\int dq J(\boldsymbol{q})\, \boldsymbol{m}(\boldsymbol{q}) \cdot \boldsymbol{m}(-\boldsymbol{q}) \tag{7}$$

in the momentum space, with

$$\begin{aligned} J(\boldsymbol{q}) = &-2J_1(\cos q_x + \cos q_y) \\ &-2J_2(\cos(q_x - q_y) + \cos(q_x + q_y)) \\ &-2J_3(\cos 2q_x + \cos 2q_y). \end{aligned} \tag{8}$$

The Hamiltonian has the following three symmetries:
1) the inversion symmetry: $q_x \longmapsto -q_x,\ q_y \longmapsto -q_y$;
2) the x-reflection symmetry: $q_x \longmapsto -q_x,\ q_y \longmapsto q_y$;
3) the y-reflection symmetry: $q_x \longmapsto q_x,\ q_y \longmapsto -q_y$.
It is convenient to define the vorticity number Q_v by the winding number of the in-plane spin texture, namely

$$Q_\mathrm{v} = \frac{1}{2\pi}\oint_C d\phi = \frac{1}{2\pi}[\phi]_{\varphi=0}^{\varphi=2\pi}. \tag{9}$$

We consider the transformation $Q_v \longmapsto -Q_v$ and $\eta \longmapsto -\eta$, under which the skyrmion number is inverted, $Q \longmapsto -Q$. In this symmetry operation, the spins are mapped to

$$m_x \longmapsto m_x, \qquad m_y \longmapsto -m_y, \qquad m_z \longmapsto m_z. \tag{10}$$

The Hamiltonian is invariant with the above transformation. As a result, a skyrmion with Q_v and η and an antiskyrmion

with $-Q_v$ and $-\eta$ have the same energy. Moreover, we can show that the energy is independent of η analytically.

The Taylor expansion of the Hamiltonian equation (7) reads

$$J(\boldsymbol{q}) \simeq -4(J_1+J_2+J_3)+(J_1+2J_2+4J_3)\left(q_x^2+q_y^2\right) - \left(\frac{J_1}{12}+\frac{J_2}{6}+\frac{4J_3}{3}\right)\left(q_x^4+q_y^4\right)-J_2q_x^2q_y^2. \tag{11}$$

We chose the values of J_1, J_2 and J_3, which satisfy $J_1+J_2+J_3>0$ and $\frac{J_1}{12}+\frac{J_2}{6}+\frac{4J_3}{3}<0$. When $J_1+J_2+J_3<0$, the skyrmion is not stabilized since q^4 terms do not play an important role. The condition $\frac{J_1}{12}+\frac{J_2}{6}+\frac{4J_3}{3}<0$ is necessary to cut the expansion with the order of q^4.

In the polar coordinate, substituting

$$q_x=\cos\theta\frac{\partial}{\partial r}-\frac{1}{r}\sin\theta\frac{\partial}{\partial\theta}, \qquad q_y=\sin\theta\frac{\partial}{\partial r}+\frac{1}{r}\cos\theta\frac{\partial}{\partial\theta}, \tag{12}$$

the Hamiltonian is rewritten as

$$\begin{aligned} H=\int rdr\Bigg[&-8\pi(J_1+J_2+J_3)+2\pi(J_1+2J_2+4J_3)\left(\theta'(r)^2+\frac{n^2}{r^2}\sin^2\theta(r)\right)+\\ &-\left(\frac{J_1}{12}+\frac{J_2}{6}+\frac{4J_3}{3}\right)\Bigg\{\frac{3\pi}{2}\left(\theta''(r)^2+\theta'(r)^4+\frac{n^2+1}{r^2}\theta'(r)^2\right)+\frac{\pi}{r}\theta'(r)\theta''(r)+\frac{n^2\pi\left(4+3n^2\right)}{2r^4}\sin^2\theta(r)\\ &+\frac{n^2\pi\sin 2\theta(r)}{2r^2}\left(7\theta'(r)+\theta''(r)\right)+\frac{n^2\pi\cos 2\theta(r)}{2r^2}\theta'(r)^2\Bigg\}\\ &-J_2\Bigg\{\frac{\pi}{4}\left(\theta''(r)^2+\theta'(r)^4+\frac{n^2+1}{r^2}\theta'(r)^2\right)-\frac{\pi}{2r}\theta'(r)\theta''(r)+\frac{n^2\left(4+n^2\right)}{4r^4}\sin^2\theta(r)\\ &+\frac{n^2\pi\sin 2\theta(r)}{4r^2}\left(5\theta'(r)+\theta''(r)\right)+\frac{3n^2\pi\cos 2\theta(r)}{4r^2}\theta'(r)^2\Bigg\}\Bigg]. \end{aligned} \tag{13}$$

This is independent of η, which implies that the energy is independent of the helicity. Furthermore, the Hamiltonian is invariant for $n\longmapsto -n$, which implies the energy between the skyrmion and the antiskyrmion is identical irrespective to the helicity η.

* These authors contributed equally to this work.
† E-mail: zhouyan@cuhk.edu.cn
‡ E-mail: ezawa@ap.t.u-tokyo.ac.jp

[1] A. N. Bogdanov and D. A. Yablonskii, Sov. Phys. JETP **68**, 101 (1989).
[2] A. Bogdanov and A. Hubert, J. Magn. Magn. Mater. **138**, 255 (1994).
[3] U. K. Roszler, A. N. Bogdanov, and C. Pfleiderer, Nature **442**, 797 (2006).
[4] N. Nagaosa and Y. Tokura, Nat. Nano. **8**, 899 (2013).
[5] H.-B. Braun, Adv. Phys. **61**, 1 (2012).
[6] Y.-H. Liu and Y.-Q. Li, Chin. Phys. B **24**, 17506 (2015).
[7] R. Wiesendanger, Nat. Rev. Mat. **1**, 16044 (2016).
[8] W. Kang, Y. Huang, X. Zhang, Y. Zhou, and W. Zhao, Proc. IEEE **104**, 2040 (2016).
[9] G. Finocchio, F. Büttner, R. Tomasello, M. Carpentieri, and M. Kläui, J. Phys. D: Appl. Phys. **49**, 423001 (2016).
[10] S. Seki and M. Mochizuki, *Skyrmions in Magnetic Materials* (Springer, Switzerland, 2016).
[11] W. Jiang, W. Zhang, G. Yu, M. B. Jungfleisch, P. Upadhyaya, H. Somaily, J. E. Pearson, Y. Tserkovnyak, K. L. Wang, O. Heinonen, S. G. E. te Velthuis, and A. Hoffmann, AIP Adv. **6**, 055602 (2016).
[12] S. Mühlbauer, B. Binz, F. Jonietz, C. Pfleiderer, A. Rosch, A. Neubauer, R. Georgii, and P. Böni, Science **323**, 915 (2009).
[13] X. Z. Yu, Y. Onose, N. Kanazawa, J. H. Park, J. H. Han, Y. Matsui, N. Nagaosa, and Y. Tokura, Nature **465**, 901 (2010).
[14] S. Heinze, K. von Bergmann, M. Menzel, J. Brede, A. Kubetzka, R. Wiesendanger, G. Bihlmayer, and S. Blugel, Nat. Phys. **7**, 713 (2011).
[15] N. Romming, C. Hanneken, M. Menzel, J. E. Bickel, B. Wolter, K. von Bergmann, A. Kubetzka, and R. Wiesendanger, Science **341**, 636 (2013).
[16] H. Du, R. Che, L. Kong, X. Zhao, C. Jin, C. Wang, J. Yang, W. Ning, R. Li, C. Jin, X. Chen, J. Zang, Y. Zhan, and M. Tian, Nat. Commun. **6**, 8504 (2015).
[17] A. Bogdanov and A. Hubert, Nat. Commun. **6**, 8539 (2015).
[18] F. Buttner, C. Moutafis, M. Schneider, B. Kruger, C. M. Gunther, J. Geilhufe, C. v. K. Schmising, J. Mohanty, B. Pfau, S. Schaffert,

A. Bisig, M. Foerster, T. Schulz, C. A. F. Vaz, J. H. Franken, H. J. M. Swagten, M. Klaui, and S. Eisebitt, Nat. Phys. **11**, 225 (2015).
[19] W. Jiang, P. Upadhyaya, W. Zhang, G. Yu, M. B. Jungfleisch, F. Y. Fradin, J. E. Pearson, Y. Tserkovnyak, K. L. Wang, O. Heinonen, S. G. E. te Velthuis, and A. Hoffmann, Science **349**, 283 (2015).
[20] S. Woo, K. Litzius, B. Kruger, M.-Y. Im, L. Caretta, K. Richter, M. Mann, A. Krone, R. M. Reeve, M. Weigand, P. Agrawal, I. Lemesh, M.-A. Mawass, P. Fischer, M. Klaui, and G. S. D. Beach, Nat. Mater. **15**, 501 (2016).
[21] X. Z. Yu, N. Kanazawa, Y. Onose, K. Kimoto, W.Z. Zhang, S. Ishiwata, Y. Matsui, and Y. Tokura, Nat. Mater. **10**, 106 (2011).
[22] T. Schulz, R. Ritz, A. Bauer, M. Halder, M. Wagner, C. Franz, C. Pfleiderer, K. Everschor, M. Garst, and A. Rosch, Nat. Phys. **8**, 301 (2012).
[23] H. Oike, A. Kikkawa, N. Kanazawa, Y. Taguchi, M. Kawasaki, Y. Tokura, and F. Kagawa, Nat. Phys. **12**, 62 (2016).
[24] W. Jiang, X. Zhang, G. Yu, W. Zhang, X. Wang, M. B. Jungfleisch, J. E. Pearson, X. Cheng, O. Heinonen, K. L. Wang, Y. Zhou, A. Hoffmann, and S. G. E. te Velthuis, Nat. Phys. **13**, 162 (2017).
[25] H. Du, J. P. DeGrave, F. Xue, D. Liang, W. Ning, J. Yang, M. Tian, Y. Zhang, and S. Jin, Nano Lett. **14**, 2026 (2014).
[26] I. Kezsmarki, S. Bordacs, P. Milde, E. Neuber, L. M. Eng, J. S. White, H. M. Ronnow, C. D. Dewhurst, M. Mochizuki, K. Yanai, H. Nakamura, D. Ehlers, V. Tsurkan, and A. Loidl, Nat. Mater. **14**, 1116 (2015).
[27] S. Seki, X. Z. Yu, S. Ishiwata, and Y. Tokura, Science **336**, 198 (2012).
[28] Y. Nahas, S. Prokhorenko, L. Louis, Z. Gui, I. Kornev, and L. Bellaiche, Nat. Commun. **6**, 8542 (2015).
[29] G. Yu, P. Upadhyaya, Q. Shao, H. Wu, G. Yin, X. Li, C. He, W. Jiang, X. Han, P. K. Amiri, and K. L. Wang, Nano Lett. **17**, 261 (2017).
[30] A. Fert, V. Cros, and J. Sampaio, Nat. Nano. **8**, 152 (2013).
[31] J. Sampaio, V. Cros, S. Rohart, A. Thiaville, and A. Fert, Nat. Nano. **8**, 839 (2013).
[32] J. Iwasaki, M. Mochizuki, and N. Nagaosa, Nat. Nano. **8**, 742 (2013).
[33] R. Tomasello, E. Martinez, R. Zivieri, L. Torres, M. Carpentieri, and G. Finocchio, Sci. Rep. **4**, 6784 (2014).
[34] Y. Zhou and M. Ezawa, Nat. Commun. **5**, 4652 (2014).
[35] X. Zhang, Y. Zhou, and M. Ezawa, Nat. Commun. **7**, 10293 (2016).
[36] W. Koshibae, Y. Kaneko, J. Iwasaki, M. Kawasaki, Y. Tokura, and N. Nagaosa, J. J. Appl. Phys. **54**, 053001 (2015).
[37] M. Beg, R. Carey, W. Wang, D. Cortes-Ortuno, M. Vousden, M.-A. Bisotti, M. Albert, D. Chernyshenko, O. Hovorka, R. L. Stamps, and H. Fangohr, Sci. Rep. **5**, 17137 (2015).
[38] X. Zhang, G. P. Zhao, H. Fangohr, J. P. Liu, W. X. Xia, J. Xia, and F. J. Morvan, Sci. Rep. **5**, 7643 (2015).
[39] D. Bazeia, J. G. G. S. Ramos, and E. I. B. Rodrigues, J. Magn. Magn. Mater. **423**, 411 (2017).
[40] C. Navau, N. Del-Valle, and A. Sanchez, Phys. Rev. B **94**, 184104 (2016).
[41] Z. Wang and M. J. Grimson, Phys. Rev. B **94**, 14311 (2016).
[42] L. Sun, R. X. Cao, B. F. Miao, Z. Feng, B. You, D. Wu, W. Zhang, A. Hu, and H. F. Ding, Phys. Rev. Lett. **110**, 167201 (2013).
[43] W. Koshibae and N. Nagaosa, Nat. Commun. **5**, 5148 (2013).
[44] C. Reichhardt, D. Ray, and C. J. Olson Reichhardt, New J. Phys. **17**, 073034 (2015).
[45] X. Zhang, M. Ezawa, and Y. Zhou, Sci. Rep. **5**, 9400 (2015).
[46] Y. Zhou, E. Iacocca, A. A. Awad, R. K. Dumas, F. C. Zhang, H. B. Braun, and J. Akerman, Nat. Commun. **6**, 8193 (2015).
[47] S. Zhang, J. Wang, Q. Zheng, Q. Zhu, X. Liu, S. Chen, C. Jin, Q. Liu, C. Jia, and D. Xue, New J. Phys. **17**, 023061 (2015).
[48] Y. Dai, H. Wang, T. Yang, W. Ren, and Z. Zhang, Sci. Rep. **4**, 6153 (2014).
[49] X. Zhang, M. Ezawa, D. Xiao, G. P. Zhao, Y. Liu, and Y. Zhou, Nanotechnology **26**, 225701 (2015).
[50] X. Zhang, Y. Zhou, M. Ezawa, G. P. Zhao, and W. Zhao, Sci. Rep. **5**, 11369 (2015).
[51] P. Upadhyaya, G. Yu, P. K. Amiri, and K. L. Wang, Phys. Rev. B **92**, 134411 (2015).
[52] S.-Z. Lin and S. Hayami, Phys. Rev. B **93**, 064430 (2016).
[53] A. O. Leonov and M. Mostovoy, Nat. Commun. **6**, 8275 (2015).
[54] A. O. Leonov and M. Mostovoy, Nat. Commun. **8**, 14394 (2017).
[55] S. Hayami, S.-Z. Lin, and C. D. Batista, Phys. Rev. B **93**, 184413 (2016).
[56] C. D. Batista, S.-Z. Lin, S. Hayami, and Y. Kamiya, Rep. Prog. Phys. **79**, 84504 (2016).
[57] S.-Z. Lin, S. Hayami, and C. D. Batista, Phys. Rev. Lett. **116**, 187202 (2016).
[58] S. Hayami, S.-Z. Lin, Y. Kamiya, and C. D. Batista, Phys. Rev. B **94**, 174420 (2016).
[59] H. Y. Yuan, O. Gomonay, and M. Kläui, arXiv:1610.02172.
[60] T. H. R. Skyrme, Proc. Roy. Soc. A **260**, 127 (1961).
[61] X. Zhang, Y. Zhou, and M. Ezawa, Phys. Rev. B **93**, 024415 (2016).
[62] W. Koshibae and N. Nagaosa, Nat. Commun. **7**, 10542 (2016).
[63] M. J. Donahue and D. G. Porter, OOMMF User's Guide, Interagency Report NISTIR 6376, NIST, Gaithersburg, MD, 1999, http://math.nist.gov/oommf.

Acknowledgments
X.Z. was supported by JSPS RONPAKU (Dissertation Ph.D.) Program. X.Z. is grateful to W. Jiang for many useful comments. X.Z. also thanks S.-Z. Lin for discussions on frustrated skyrmions. Y.Z. acknowledges the support by the National Natural Science Foundation of China (Project No. 11574137) and Shenzhen Fundamental Research Fund under Grant No. JCYJ20160331164412545. M.E. acknowledges the support by the Grants-in-Aid for Scientific Research from JSPS KAKENHI (Grant Nos. 25400317 and 15H05854), and also the support by CREST, JST. M.E. is very much grateful to N. Nagaosa for many helpful discussions on the subject.

Author contributions
M.E. and Y.Z. conceived the idea. Y.Z., X.L., and M.E. coordinated the project. X.Z. performed the numerical simulation and data analysis. J.X. developed the modules for NNN and NNNN exchange interactions. M.E. carried out the theoretical analysis. All authors interpreted the results and prepared the manuscript.

Additional information
Supplementary information is available in the online version of the paper. Correspondence and requests for materials should be addressed to M.E. and Y.Z.

Competing financial interests
The authors declare no competing financial interests.